Article

Phomopsichin A–D; Four New Chromone Derivatives from Mangrove Endophytic Fungus *Phomopsis* sp. 33#

Meixiang Huang [1,†]**, Jing Li** [2,3,†]**, Lan Liu** [2,4,*]**, Sheng Yin** [1]**, Jun Wang** [1,*] **and Yongcheng Lin** [3,4,5]

[1] School of Pharmaceutical Sciences, Sun Yat-sen University, Guangzhou 510006, China;
    huangmx7@mail2.sysu.edu.cn (M.H.); yinsh2@mail.sysu.edu.cn (S.Y.)
[2] School of Marine Sciences, Sun Yat-sen University, Guangzhou 510006, China; lijing356@mail.sysu.edu.cn
[3] Key Laboratory of Functional Molecules from Oceanic Microorganisms (Sun Yat-sen University),
    Department of Education of Guangdong Province, Guangzhou 510080, China
[4] South China Sea Bio-Resource Exploitation and Utilization Collaborative Innovation Center,
    Guangzhou 510006, China
[5] School of Chemistry and Chemical Engineering, Sun Yat-sen University, Guangzhou 510275, China;
    ceslyc@mail.sysu.edu.cn
* Correspondence: cesllan@mail.sysu.edu.cn (L.L); wjun@mail.sysu.edu.cn (J.W.);
    Tel.: +86-208-411-4834 (L.L.); +86-203-994-3090 (J.W.)
† These authors contributed equally to this work.

Abstract: Four new chromone derivatives, phomopsichins A–D (**1**–**4**), along with a known compound, phomoxanthone A (**5**), were isolated from the fermentation products of mangrove endophytic fungus *Phomopsis* sp. 33#. Their structures were elucidated based on comprehensive spectroscopic analysis coupled with single-crystal X-ray diffraction or theoretical calculations of electronic circular dichroism (ECD). They feature a tricyclic framework, in which a dihydropyran ring is fused with the chromone ring. Compounds **1**–**5** showed weak inhibitory activities on acetylcholinesterase as well as α-glucosidase, weak radical scavenging effects on 1,1-diphenyl-2-picrylhydrazyl (DPPH) as well as OH, and weak antimicrobial activities. Compounds **1**–**4** showed no cytotoxic activity against MDA-MB-435 breast cancer cells. Their other bioactivities are worthy of further study, considering their unique molecular structures.

Keywords: mangrove endophytic fungi; *Phomopsis* sp.; secondary metabolites; chromone derivatives

1. Introduction

The chromone family of natural products exhibit a range of biological activities including anticancer, anti-inflammatory, antibacterial, antiviral, atypical antipsychotic, and anti-platelet properties [1–9]. In our continuous investigation of new bioactive secondary metabolites from the mangrove endophytic fungi in the South China Sea, four new chromone derivatives, phomopsichin A–D (**1**–**4**), along with a known compound, phomoxanthone A (**5**), were isolated from the metabolic products of endophytic fungus *Phomopsis* sp. 33# from the bark of the mangrove plant *Rhizophora stylosa*. Compounds **1**–**3** (Figure 1) featured a tricyclic framework in which a dihydropyran ring is fused at C-3 and C-4 of the chromone ring. To our knowledge, the compounds with this type skeleton number approximately 10, which were reported to exhibit the activity attenuating resistin-induced adhesion of HCT-116 colorectal cancer cells to endothelial cells [10], the activity interrupting the dimer formation of Aβ17–42 peptide associated to Alzheimer's disease [11], inhibitory activity against metallo-β-lactamases [12], moderate antibacterial activity and weak cytotoxic activity [13–15]. In this study, we report the isolation, structural elucidation, and exploration on the biological activities of compounds **1**–**5**.
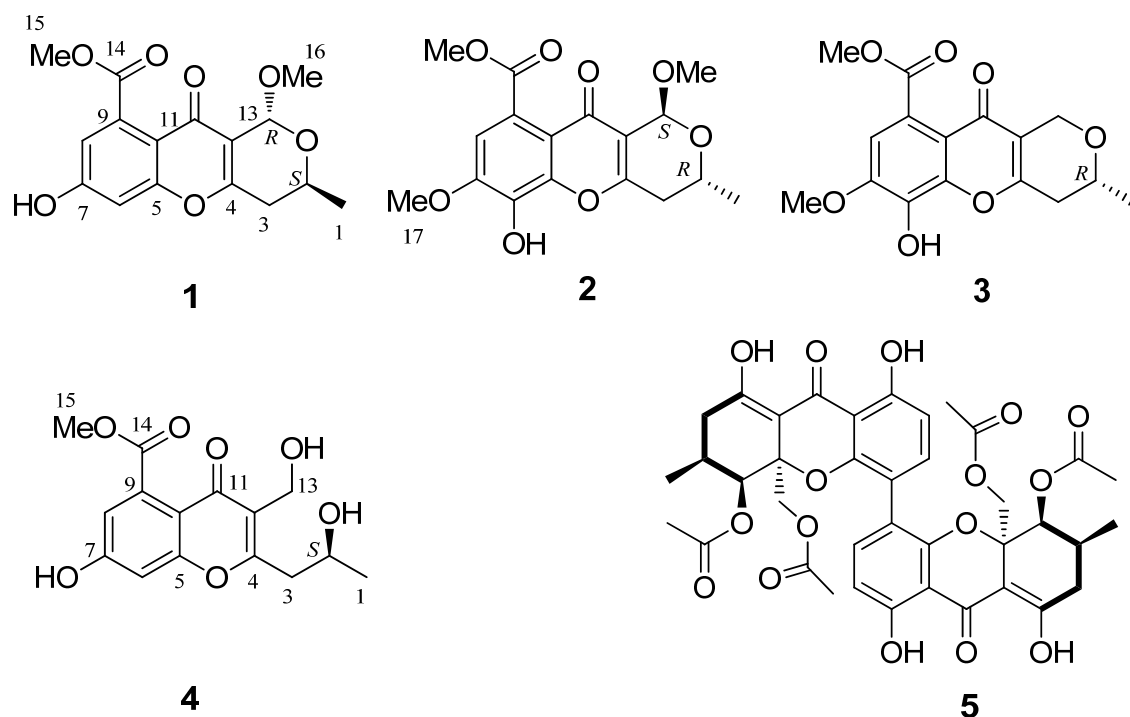
**Figure 1.** The chemical structures of compounds **1**–**5**.

2. Results

2.1. Structure Elucidation

Phomopsichin A (**1**, Figure 1) was obtained as a white solid and had a molecular formula of $C_{16}H_{16}O_7$ as determined by its datum of high resolution electrospray ionization mass spectroscopy (HRESIMS) (observed *m/z* 319.08184 M$^-$, calculated 319.08233), requiring nine degrees of unsaturation. The ^{13}C-NMR and distortionless enhancement by polarization transfer (DEPT) spectra (Table 1) indicated the presence of two carbonyl groups (δ_c 169.5 and 173.2), eight olefinic carbons, two sp^3 CH groups, one sp^3 CH$_2$ group, two methoxy groups, and one methyl group. The ^{1}H-NMR and ^{1}H-^{1}H correlation spectroscopy (COSY) (Table 1 and Figure 2) showed the signals of two *m*-hydrogens of phenol (δ_H 6.93 d *J* = 2.4 Hz; 6.85 d *J* = 2.4 Hz), two methoxy groups (δ_H 3.85/3.42), and one 2-oxo-propyl group (δ_H 1.34 d *J* = 6.0 Hz; 4.34 m; 2.67 dd *J* = 18.0, 4.0 Hz; 2.58 dd *J* = 18.0, 4.0 Hz). The remaining two degrees of unsaturation supported a tricyclic carbon framework of dihydropyrano[4,3-b]chromen-10(1H)-one in **1**, which was confirmed by the correlations between H-13 and C-2/C-11 in heteronuclear multiple-bond correlation (HMBC) spectroscopy. In the HMBC spectrum (Figure 2), rich correlation data allowed us to unambiguously establish the locations of substituents on the carbon skeleton. The HMBC correlation between H-8 and C-14 revealed that the carbonyl group was located at the C-9 position; the correlation between H$_3$-1 and C-3 demonstrated that the CH$_3$-1 was located at the C-2 position; and the correlations between H$_3$-15 and C-14 as well as between H$_3$-16 and C-13 indicated that the two methoxy groups were located at the C-14 and C-13 positions, respectively. One hydroxyl group was identified at the C-7 position based on the lower field chemical shift (δ_c 162.6, C-7).

Table 1. ^{1}H-NMR and ^{13}C-NMR data of compounds **1–4** (400/100 MHz, *J* in Hz).

	1 (in C$_3$D$_6$O)		2 (in CDCl$_3$)		3 (in CDCl$_3$)		4 (in CD$_3$OD)	
	δ_C	δ_H	δ_C	δ_H	δ_C	δ_H	δ_C	δ_H
1	21.0 q	1.34 d 6.0	21.0 q	1.39 d 6.4	21.3 q	1.38 d 6.0	23.8 q	1.31 d 6.0
2	62.8 d	4.34 m	62.1 d	4.41 m	70.0 d	3.83 m	66.7 t	4.23 m
3	34.6 t	2.67 dd 18.0, 4.0 2.58 dd 18.0,10.8	34.4 t	2.63 m	34.6 t	2.64 m	42.1 t	2.94 m
4	164.1 s		163.6 s		160.7 s		167.7 s	
5	158.4 s		144.4 s		144.8 s		159.3 s	
6	104.3 d	6.93 d 2.4	134.7 s		134.9 s		104.4 d	6.87 d 2.4
7	162.6 s		149.2 s		149.0 s		164.2 s	
8	113.8 d	6.85 d 2.4	108.0 d	6.89 s	107.9 d	6.93 s	114.8 d	6.77 d 2.4
9	114.6 s		124.5 s		124.0 s		113.7 s	
10	136.4 s		116.0 s		115.6 s		136.2 s	
11	173.2 s		173.5 s		174.1 s		177.2 s	
12	117.4 s		116.6 s		116.5 s		122.1 s	
13	95.2 d	5.40 s	94.5 d	5.57 s	62.5 t	4.82 d 15.2 4.48 d 15.2	55.0 t	4.55 s
14	169.5 s		169.8 s		170.0 s		171.6 s	
15	52.8 q	3.85 s	53.2 q	3.95 s	53.2 q	3.96 s	53.3 q	3.91 s
16	55.6 q	3.42 s	55.9 q	3.55 s				
17			56.8 q	3.98 s	56.9 q	3.99 s		
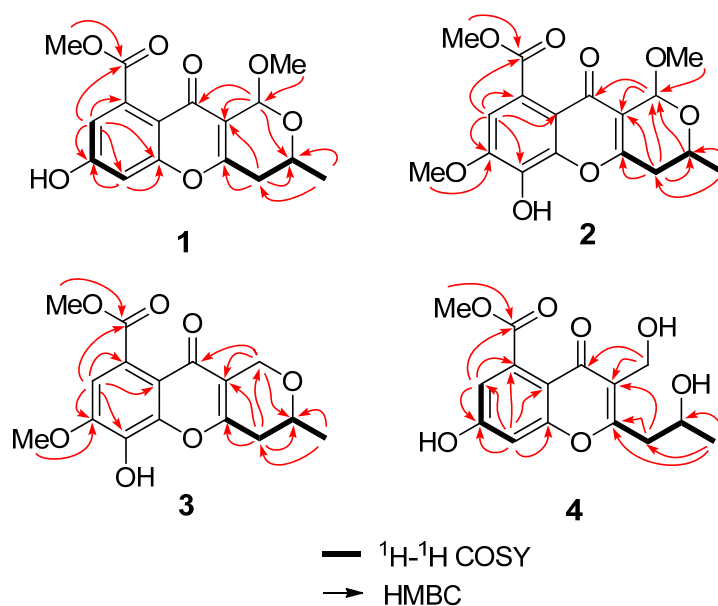
Figure 2. The key ^{1}H-^{1}H COSY and HMBC correlations of compounds **1–4**.

The relative stereochemistry of **1** was established by its nuclear Overhauser effect spectroscopy (NOESY). The NOE correlation between H-2 and H$_3$-16 indicated the relative stereochemistry of **1** as shown in Figure 3.

The complete structure and stereochemistry of **1** were further confirmed by X-ray diffraction analysis (Figure 4). The final refinement of the Cu Kα data resulted in a small Flack parameter of 0.02(3), allowing an unambiguous assignment of the absolute configuration of **1** as 2*S*, 13*R* (Figure 1).

Phomopsichin B (**2**, Figure 1) was obtained as a white solid and had a molecular formula of C$_{17}$H$_{18}$O$_8$ based on HRESIMS data (observed *m/z* 349.09241 M$^-$, calculated 349.09289), with one more CH$_3$O group than compound **1**. The ^{1}H-NMR, ^{13}C-NMR, and HMBC spectra of **2** were very similar to those of **1** (Table 1), except for the absence of the H-6 signal, and an added CH$_3$O-17 signals ($\delta_{H/C}$ 3.98/56.8). The added CH$_3$O-17 was located at the C-7 position based on the NOE correlation

between H-17 and H-8. One hydroxyl group was identified at the C-6 position based on the chemical shift of C-6 (δ_C 134.7) as well as the HMBC correlation between H-8 and C-6.
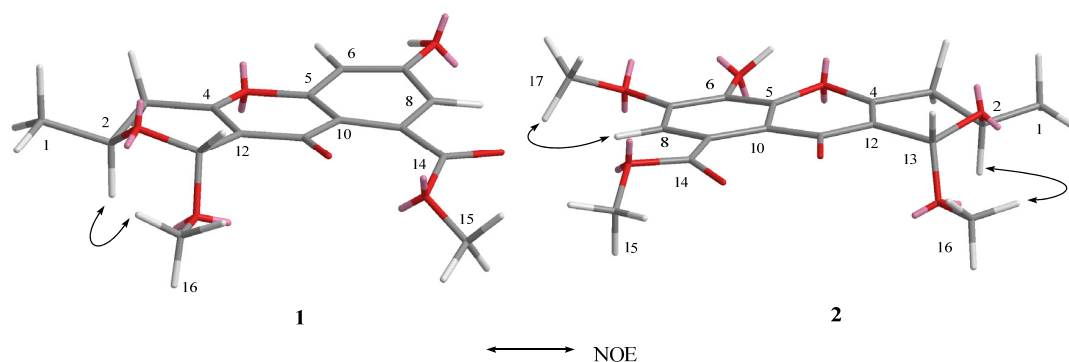

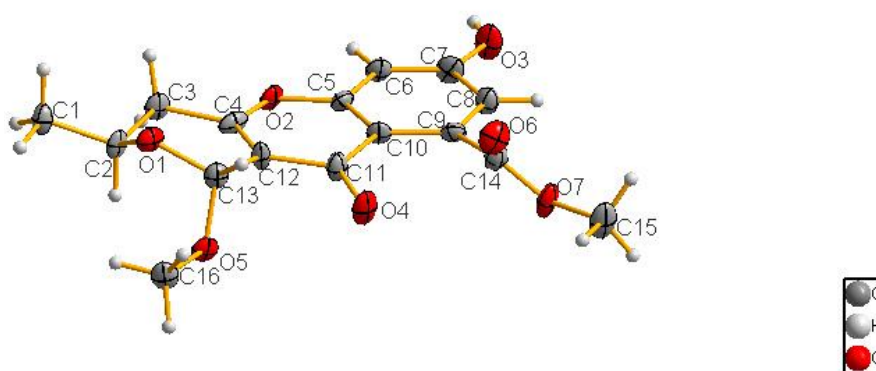**Figure 3.** The key correlations of compounds **1** and **2** in NOESY.

Figure 4. The X-ray single-crystal structure of **1**.

The relative stereochemistry of **2** was established by its NOESY. The NOE correlation between H-2 and H$_3$-16, similar to those of **1**, indicated the relative stereochemistry of **2** as shown in Figure 3.

Compounds **2** and **1** have identical chiral spheres, just opposite in the signs of their specific rotation data; their ECD spectra were symmetric (Figure 5). The ECD spectrum of **2** showed negative Cotton effect at 318 ($\Delta\varepsilon$ −0.48) nm as well as positive one at 291 ($\Delta\varepsilon$ +0.53) nm. Meanwhile, the ECD spectrum of **1** displayed opposite Cotton effects at the same wavelengths. For the above reasons, the absolute configuration of **2** was suggested as 2*R*, 13*S*.
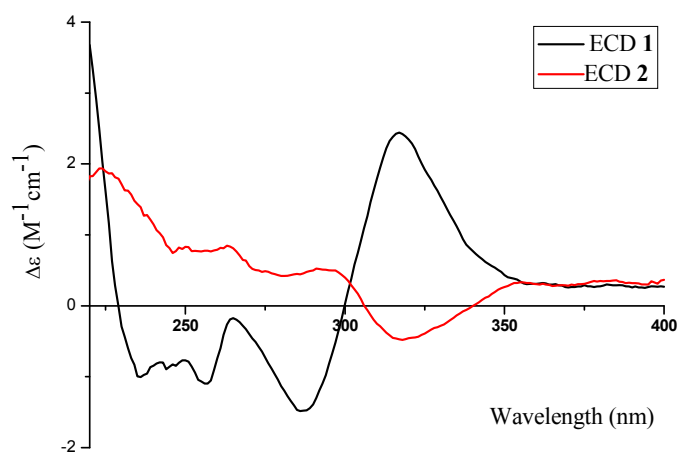

Figure 5. The ECD spectra of **1** and **2**.

Phomopsichin C (**3**, Figure 1) was obtained as a white solid and had a molecular formula of $C_{16}H_{16}O_7$ based on HRESIMS data (observed *m/z* 319.08200 M$^-$, calculated 319.08233). The ^{1}H-NMR, ^{13}C-NMR, ^{1}H-^{1}H COSY, and HMBC spectra of **3** were very similar to those of compound **2** (Table 1, Figure 2), except for the changes of CH-13 signals ($\delta_{H/C}$ 5.57/94.5) in **2** to CH_2-13 signals ($\delta_{H/C}$ 4.82 d; 4.48 d/62.5) in **3**. These results suggested that compound **3** is lacking a methoxy group at the C-13 position. The absolute configuration of compound **3** was determined as 2*R* by the result that the experimental ECD and calculated ECD spectrum for 2*R* isomer matched exactly (Figure 6).
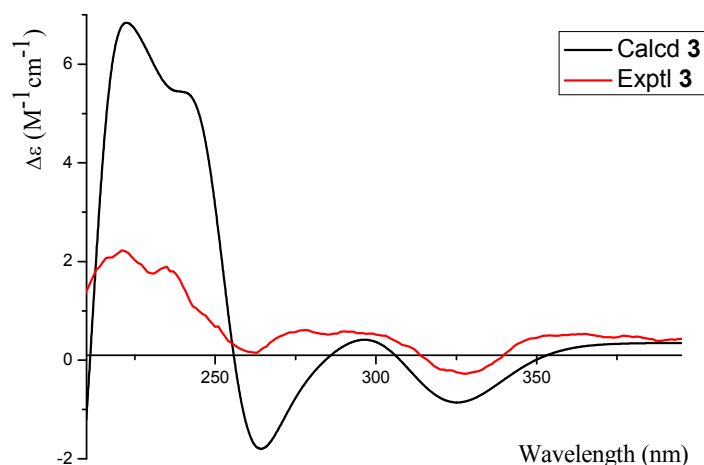

Figure 6. The calculated and experimental ECD spectra of **3**.

Phomopsichin D (**4**, Figure 1) had a molecular formula of $C_{15}H_{16}O_7$ based on HRESIMS data (observed *m/z* 307.08194 M$^-$, calculated 307.08233), requiring eight degrees of unsaturation. The ^{1}H-NMR, ^{13}C-NMR, ^{1}H-^{1}H COSY, and HMBC spectra of **4** were very similar to those of **1** (Table 1 and Figure 2), except for the change of CH-13 signals ($\delta_{H/C}$ 5.40/95.2) in **1** to CH_2OH-13 signals ($\delta_{H/C}$ 4.55/55.0) and the absence of a methoxy group signal in **4**. A dicyclic 4*H*-chromen-4-one segment of **4** was decided based on its eight degrees of unsaturation, which was supported by the absence of HMBC correlation between H-13 and C-2. The hydroxymethyl group was located at C-12 based on the HMBC correlation between H-13 and C-11. A 2-hydroxypropyl group was located at C-4 based on the HMBC correlations between H-1 and C-4, as well as, between H-3 and C-12.

The absolute configuration of **4** was confirmed as 2*S* based on the result that the experimental data and calculated ECD spectrum for the 2*S* isomer matched exactly (Figure 7).
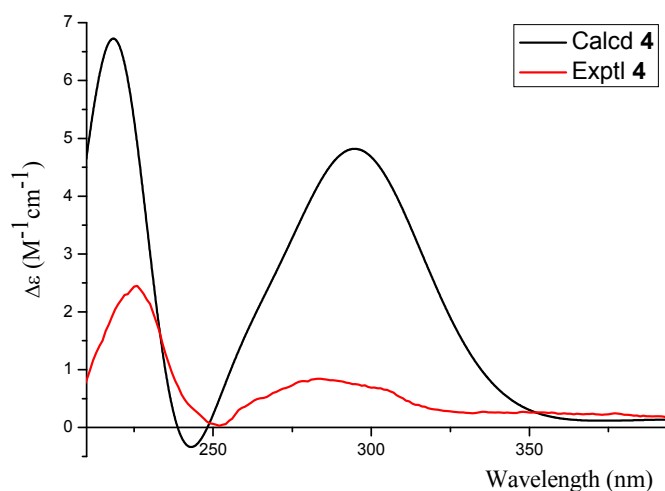

Figure 7. The calculated and experimental ECD spectra of **4**.

Compound **5** was identified as phomoxanthone A (**5**, Figure 1) by comparison of its spectral data with that of the literature [16,17]; both compound **5** and phomoxanthone A had the same NMR, MS, ECD data (Figure S27, in Supplementary Materials) and specific rotation data.

2.2. Biological Evaluation

The various bioactivities of compounds **1**–**5** were evaluated in vitro. The five compounds displayed low inhibitory activities on acetylcholinesterase (AchE) as well as α-glucosidase, weak radical scavenging effects on DPPH as well as OH, and low antimicrobial activity against 13 pathogenic bacteria strains (Tables S8 and S9, in Supplementary Materials). Compounds **1**–**4** showed no cytotoxic activity against MDA-MB-435 breast cancer cells. It was reported that phomoxanthone A (**5**) has strong pro-apoptotic activity and immunostimulatory activity [17], so we did not consider its cytotoxicity assays in the study.

3. Materials and Methods

3.1. General Experimental Procedures

Acetylcholinesterase (AchE), S-acetylthiocholine iodide, 5,5′-dithio-bis-(2-nitrobenzoic acid), huperzine A, α-glucosidase and *p*-nitrophenyl-α-D-glucopyranoside were purchased from Sigma (St. Louis, MO, USA); 1,1-diphenyl-2-picrylhydrazyl (DPPH), H_2O_2, 1,10-phenanthroline, $FeSO_4$, and other reagents were of analytical grade and commercially available; methanol was of chromatographic grade; potato dextrose agar (PDA) medium was purchased from Beijing L and Bridge Technology Co. Ltd. (Beijing, China).

Optical rotation measurements were carried out using a Bellingham-Stanley 37–440 polarimeter (Bellingham Stanley Ltd., Kent, UK). UV spectra were determined using a UV-240 spectrophotometer (Shimadzu, Tokyo, Japan). ECD spectra were measured using a Chirascan Circular Dichroism Spectrometer (Applied Photophysics, London, UK). IR spectra were measured on a TENSOR37 spectrometer (Bruker Optics, Ettlingen, Germany). The ^{1}H-NMR and ^{13}C-NMR data were acquired using a Bruker Avance 400 spectrometer at 400 MHz for ^{1}H nuclei and 100 MHz for ^{13}C nuclei (Bruker Biospin, Rheinstetten, Germany). Tetramethylsilane (TMS) was used as an internal standard, and the chemical shifts (δ) were expressed in ppm. The HRESIMS were obtained using a LTQ-Orbitrap LC-MS (Thermo Fisher, Frankfurt, Germany). Single-crystal data were carried out on an Agilent Technologies Gemini A Ultra system (Agilent Tech, Santa Clara, CA, USA). HPLC was performed using a 515 pump with a UV 2487 detector (Waters, Milford, CT, USA) and an Ultimate XB-C-18 column (250 mm × 10 mm, 5 μm; Welch, Maryland, USA). Normal pressure preparative column chromatography was carried out on RP-18 gel (25–40 μm, Daiso Inc., Osaka, Japan), silica gel (200–400 mesh, Qingdao Marine Chemical Inc., Qingdao, China), or a Sephadex-LH-20 (GE Healthcare, Stockholm, Sweden) for reverse and direct phase elution modes, respectively. The thin-layer chromatography was performed over F_{254} glass plates (Qingdao Marine Chemical Inc.) and analyzed under UV light (254 and 366 nm).

3.2. Fungal Material

Endophytic fungus *Phomopsis* sp. 33# was isolated with PDA medium from the bark of the mangrove plant *Rhizophora stylosa*, collected in the intertidal region of Zhanjiang, in Guangdong Province, China, and identified according to its morphological characteristics and internal transcribed spacer (ITS) region [18]. A voucher specimen is deposited in our laboratory at −20 °C.

3.3. Fermentation, Extraction, and Isolation

Small agar slices bearing mycelia were placed in 1000 mL Erlenmeyer flasks containing rice medium (composed of 60 g rice, 80 mL distilled water, and 0.24 g sea salt) and incubated for 30 days at 28 °C. In total, 140 flasks of culture were obtained. Cultures were extracted with EtOAc. In total,

250 g crude extract was obtained by evaporation of EtOAc. The crude extract was suspended in H_2O (3 L) and partitioned with *n*-hexane (5 L × 2) and EtOAc (5 L × 2) to give *n*-hexane (90 g) and EtOAc (110 g) extracts, respectively.

The EtOAc extract was subjected to a silica gel column, eluted with a *n*-hexane-EtOAc gradient (from 100:0 to 0:100) to obtain six fractions (Fractions 1–6). Fraction 2 (15 g) was extracted with 300 mL of chloroform to give dark yellow liquid phases and solid. The chloroform-soluble fraction was evaporated to dryness and washed with methanol (50 mL × 6) to give compound **5** (a light yellow solid, 5.2 g). Fraction 4 (15 g) was chromatographed over a column of RP-18 gel (2.5 cm × 30 cm, MeOH-H_2O gradient from: 100:0 to 40:60) to obtain five fractions (Fractions 4.1–4.5). Fraction 4.1 and 4.3–4.5 were separated by HPLC (MeOH-H_2O, 20:80, 2 mL/min, 254 nm), respectively, and then were purified separately using a Sephadex LH-20 column (MeOH) until pure compound **1** (17 mg), compound **2** (17mg), compound **3** (10 mg), and compound **4** (22 mg) were obtained.

3.4. Spectral Data

Phomopsichin A (**1**): white solid; $[a]_D^{25}$ +12.5 (*c* 0.48, MeOH); UV (MeOH) λ_{max} (logε) 290 (4.0), 218 (4.4) nm; ECD (MeOH) λ_{max} ($\Delta\varepsilon$) 312 (+2.4), 281 (−1.5), 231 (−1.0) nm; IR (KBr) ν_{max} 3410, 2925, 1655 cm^{-1}; for ^{1}H-NMR and ^{13}C-NMR data, see Table 1; ESIMS *m/z* 319.0 [M$^-$]; HRESIMS *m/z* 319.08184 [M$^-$] (calculated for $C_{16}H_{15}O_7$, 319.08233).

Crystal structure determination of phomopsichin A (**1**): crystal data for $C_{16}H_{16}O_7$ (*M* = 320.29 g/mol): monoclinic, space group P2$_1$ (no. 4), *a* = 7.6234 (9) Å, *b* = 15.5426 (17) Å, *c* = 12.4889 (13) Å, β = 96.241 (10)°, *V* = 1471.0 (3) Å^3, Z = 4, *T* = 150 (2) K, μ (CuKα) = 0.973 mm^{-1}, *D*calc = 1.446 g/cm^3, 15,309 reflections measured (7.12° ≤ 2Θ ≤ 133.92°), 5018 unique (R_{int} = 0.0877, R$_{sigma}$ = N/A) which were used in all calculations. The final R_1 was 0.0849 (>2sigma(I)) and *wR*$_2$ was 0.2334 (all data). The crystallographic data of **1** have been deposited at the Cambridge Crystallographic Data Centre (CCDC), CCDC Depository Request CRM: 0001000638303.

Phomopsichin B (**2**): white solid; $[a]_D^{25}$ −8.0 (*c* 0.89, MeOH); UV (MeOH) λ_{max} (logε) 299 (3.8), 238 (4.4) nm; ECD (MeOH) λ_{max} ($\Delta\varepsilon$) 318 (−0.48), 291 (+0.53) nm; IR (KBr) ν_{max} 3284, 2922, 1649 cm^{-1}; for ^{1}H-NMR and ^{13}C-NMR data, see Table 1; ESIMS *m/z* 349.0 [M$^-$]; HRESIMS *m/z* 349.09241 [M$^-$] (calculated for $C_{17}H_{17}O_8$, 349.09289).

Phomopsichin C (**3**): white solid; $[a]_D^{25}$ −72 (*c* 0.05, MeOH); UV (MeOH) λ_{max} (logε) 303 (3.9), 239 (4.5) nm; ECD (MeOH) λ_{max} ($\Delta\varepsilon$) 328 (−0.27), 278 (+0.61), 221 (+2.2) nm; IR (KBr) ν_{max} 3325, 2922, 1665 cm^{-1}; for ^{1}H-NMR and ^{13}C-NMR data, see Table 1; ESIMS *m/z* 319.1 [M$^-$], 206, 175; HRESIMS *m/z* 319.08200 [M$^-$] (calculated for $C_{16}H_{15}O_7$, 319.08233).

Phomopsichin D (**4**): white solid; $[a]_D^{25}$ +102 (*c* 0.05, MeOH); UV (MeOH) λ_{max} (logε) 293 (3.8), 221 (4.2) nm; ECD (MeOH) λ_{max} ($\Delta\varepsilon$) 284 (+0.83), 226 (+2.4) nm; IR (KBr) ν_{max} 3265, 2912, 1707 cm^{-1}; for ^{1}H-NMR and ^{13}C-NMR data, see Table 1; ESIMS *m/z* 307.0 [M$^-$]; HRESIMS *m/z* 307.08194 [M$^-$] (calculated for $C_{15}H_{15}O_7$, 307.08233).

3.5. Computational Analyses

All of the theoretical methods and the basis set used for optimization and spectrum calculation were recommended in previous studies [19,20]. All of the theoretical calculations, including geometry optimization, frequency analysis, and ECD spectrum prediction, were carried out with the density functional theory (DFT) and time-dependent density functional theory (TDDFT) methods in the Gaussian 09 software package (Gaussian Inc., Wallingford, CT, USA) [21]. The geometry optimizations were performed at the B3LYP/6-31+G (d) level in the gas phase. Based on the final optimized structure, the ECD spectra were calculated at the PBE1PBE-SCRF/6-311++g (d, p) level using the Polarized Continuum Model (PCM) with methanol as a solvent. The theoretical predicted ECD spectra were fitted in the SpecDis 1.6 software package (University of Würzburg, Würzburg, Germany) [22].

3.6. X-ray Crystallographic Analysis of Compound **1**

Single crystals of compound **1** were obtained from CH_3OH-EtOAc. A suitable crystal was selected and all crystallographic data were collected at 150 K with Cu/Kα radiation (λ = 1.54178 Å). Using Olex2 (OlexSys Ltd., Durham University, Durham, UK), the structure was solved with the SIR2004 structure solution program using direct methods and refined with the XL refinement package using least squares minimization [23–25].

3.7. AchE Inhibitory Assay

The inhibitory activities against AchE of compounds **1–5** were investigated in vitro using the modified Ellman method [26]. The substrates were *S*-acetylthiocholine iodide and 5,5'-dithio-bis-(2-nitrobenzoic acid). Huperzine A was used as a positive control.

3.8. DPPH Radical Scavenging Assay

The radical scavenging effect on DPPH of compounds **1–5** were determined according to previously reported methods [27,28], and 2,6-ditertbutyl-4-methylphenol was used as a positive control.

3.9. OH-Radical-Scavenging Assay

Radical scavenging effect on OH of compounds **1–5** were carried out according to previously reported methods [29,30]. The indicator used was 1,10-phenanthroline-Fe^{2+}; vitamin C was used as a positive control.

3.10. α-Glucosidase Inhibitory Assay

The inhibitory activities against α-glucosidase of compounds **1–5** were investigated in vitro using the modified method described by Moradi-Afrapoli et al. [31]; *p*-nitrophenyl-α-D-glucopyranoside was used as the substrates, and *trans*-resveratrol was used as a positive control.

3.11. Antibacterial Experiment

The antibacterial activity of compounds **1–5** were investigated in vitro using the modified 96 well microtiter-based method described by Pierce et al. [32].

4. Conclusions

Mangrove endophytic fungi from the South China Sea provide rich fungal diversity, and are promising sources of structurally-unprecedented bioactive natural products [33–37]. Five chromone derivatives were isolated from the mangrove endophytic fungus *Phomopsis* sp. 33#, four of them are new compounds (**1–4**). Compounds **1–5** showed weak inhibitory activity of AchE as well as α-glucosidase, radical scavenging effects on DPPH as well as OH, and low antimicrobial activity. The compounds (**1–4**) showed no cytotoxic activity against MDA-MB-435 breast cancer cells. Their other bioactivities are worthy of further study, considering their unique tricyclic molecular structures, in which a dihydropyran ring is fused with the chromone ring.

D (**4**). Figure S23: ^{1}H-^{1}H COSY for phomopsichin D (**4**). Figure S24: HSQC for phomopsichin D (**4**). Figure S25: HMBC for phomopsichin D (**4**). Figure S26: HR mass spectrometry for phomopsichin D (**4**). Figure S27: ECD spectrometry for phomoxanthone A (**5**). Table S1: Crystal data and structure refinement for phomopsichin A (**1**). Table S2: Fractional atomic coordinates ($\times 10^4$) and equivalent isotropic displacement parameters ($\text{Å}^2 \times 10^3$) for phomopsichin A (**1**). Table S3: Anisotropic displacement parameters ($\text{Å}^2 \times 10^3$) for phomopsichin A (**1**). Table S4: Bond lengths for phomopsichin A (**1**). Table S5: Bond angles for phomopsichin A (**1**). Table S6: Torsion angles for phomopsichin A (**1**). Table S7: Hydrogen atom coordinates ($\text{Å} \times 10^4$) and isotropic displacement parameters ($\text{Å}^2 \times 10^3$) for phomopsichin A (1). Table S8: Inhibitory activities against AchE as well as α-glucosidase, and the radical scavenging effects on DPPH as well as OH of compounds **1**–**5**. Table S9: Antimicrobial activity of compounds **1**–**5**.

Author Contributions: Jun Wang and Lan Liu took charge throughout the research, structural elucidation and writing. Meixiang Huang mainly took part in the extraction and isolation. Jing Li mainly took part in the computational analyses. Sheng Yin mainly took part in biological activity assay. Yongcheng Lin mainly checked the error about structures elucidation.

Conflicts of Interest: The authors declare no conflict of interest.

References

1. Tang, Y.; Ling, J.; Zhang, P.; Zhang, X.; Zhang, N.; Wang, W.; Li, J.; Li, N. Potential therapeutic agents for circulatory diseases from *Bauhinia glauca* Benth.subsp. *pernervosa* (Da Ye Guan Men). *Bioorg. Med. Chem. Lett.* **2015**, *25*, 3217–3220. [CrossRef] [PubMed]

2. Hutter, J.A.; Salman, M.; Stavinoha, W.B.; Satsangi, N.; Williams, R.F.; Streeper, R.T.; Weintraub, S.T. Antiinflammatory C-glucosyl chromone from *Aloe barbadensis*. *J. Nat. Prod.* **1996**, *59*, 541–543. [CrossRef] [PubMed]

3. Speranza, G.; Morelli, C.F.; Tubaro, A.; Altinier, G.; Durì, L.; Manitto, P. Aloeresin I. An anti-inflammatory 5-methylchromone from cape aloe. *Planta Med.* **2005**, *71*, 79–81. [CrossRef] [PubMed]

4. Nastasă, C.M.; Duma, M.; Pîrnău, A.; Vlase, L.; Tiperciuc, B.; Oniga, O. Development of new 5-(chromene-3-yl)methylene-2,4-thiazolidinediones as antimicrobial agents. *Clujul Med.* **2016**, *89*, 122–127. [CrossRef] [PubMed]

5. Liu, H.S.; Xu, S.Q.; Cheng, M.; Chen, Y.; Xia, P.; Qian, K.; Xia, Y.; Yang, Z.Y.; Chen, C.H.; Morris-Natschke, S.L.; et al. Anti-AIDS agents 87. New bio-isosteric dicamphanoyl-dihydropyranochromone (DCP) and dicamphanoyl-khellactone (DCK) analogues with potent anti-HIV activity. *Bioorg. Med. Chem. Lett.* **2011**, *21*, 5831–5834. [CrossRef] [PubMed]

6. Zhou, T.; Shi, Q.; Chen, C.H.; Zhu, H.; Huang, L.; Ho, P.; Lee, K.H. Anti-AIDS agents 79. Design, synthesis, molecular modeling and structure-activity relationships of novel dicamphanoyl-2′,2′-dimethyldihydropyranochromone (DCP) analogs as potent anti-HIV agents. *Bioorg. Med. Chem.* **2010**, *18*, 6678–6689. [CrossRef] [PubMed]

7. Pires, A.D.; Lecerf-Schmidt, F.; Guragossian, N.; Pazinato, J.; Gozzi, G.J.; Winter, E.; Valdameri, G.; Veale, A.; Boumendjel, A.; Di Pietro, A.; et al. New, highly potent and non-toxic, chromone inhibitors of the human breast cancer resistance protein ABCG2. *Eur. J. Med. Chem.* **2016**, *122*, 291–301. [CrossRef] [PubMed]

8. Kumar, V.; Guru, S.K.; Jain, S.K.; Joshi, P.; Gandhi, S.G.; Bharate, S.B.; Bhushan, S.; Bharate, S.S.; Vishwakarma, R.A. A chromatography-free isolation of rohitukine from leaves of Dysoxylum binectariferum: Evaluation for in vitro cytotoxicity, CDK inhibition and physicochemical properties. *Bioorg. Med. Chem. Lett.* **2016**, *26*, 3457–3463. [CrossRef] [PubMed]

9. Bolós, J.; Anglada, L.; Gubert, S.; Planas, J.M.; Agut, J.; Príncep, M.; De la Fuente, N.; Sacristán, A.; Ortiz, J.A. 7-[3-(1-piperidinyl)propoxy]chromenones as potential atypical antipsychotics. 2. Pharmacological profile of 7-[3-[4-(6-fluoro-1, 2-benzisoxazol-3-yl)-piperidin-1-yl]propoxy]-3-(hydroxymeth yl)chromen-4-one (abaperidone. FI-8602). *J. Med. Chem.* **1998**, *41*, 5402–5409. [CrossRef] [PubMed]

10. Huang, W.S.; Yang, J.T.; Lu, C.C.; Chang, S.F.; Chen, C.N.; Su, Y.P.; Lee, K.C. Fulvic acid attenuates resistin-induced adhesion of HCT-116 colorectal cancer cells to endothelial cells. *Int. J. Mol. Sci.* **2015**, *16*, 29370–29382. [CrossRef] [PubMed]

11. Verma, S.; Singh, A.; Mishra, A. The effect of fulvic acid on pre- and postaggregation state of Aβ(17-42): Molecular dynamics simulation studies. *Biochim. Biophys. Acta* **2013**, *1834*, 24–33. [CrossRef] [PubMed]

12. Payne, D.J.; Hueso-Rodríguez, J.A.; Boyd, H.; Concha, N.O.; Janson, C.A.; Gilpin, M.; Bateson, J.H.; Cheever, C.; Niconovich, N.L.; Pearson, S.; et al. Identification of a series of tricyclic natural products as potent broad-spectrum inhibitors of metallo-beta-lactamases. *Antimicrob. Agents Chemother.* **2002**, *46*, 1880–1886. [CrossRef] [PubMed]

13. Lu, K.; Zhang, Y.; Li, L.; Wang, X.; Ding, G. Chaetochromones A and B, two new polyketides from the fungus *Chaetomium indicum* (CBS.860.68). *Molecules* **2013**, *18*, 10944–10952. [CrossRef] [PubMed]

14. Yuan, C.; Wang, H.Y.; Wu, C.S.; Jiao, Y.; Li, M.; Wang, Y.Y.; Wang, S.Q.; Zhao, Z.T.; Lou, H.X. Austdiol. Fulvic acid and citromycetin derivatives from an endolichenic fungus, *Myxotrichum* sp. *Phytochem. Lett.* **2013**, *6*, 662–666.

15. Lösgen, S.; Schlörke, O.; Meindl, K.; Herbst-Irmer, R.; Zeeck, A. Structure and biosynthesis of chaetocyclinones, new polyketides produced by an endosymbiotic Fungus. *Eur. J. Org. Chem.* **2007**, 2191–2196. [CrossRef]

16. Elsässer, B.; Krohn, K.; Flörke, U.; Root, N.; Aust, H.-J.; Draeger, S.; Schulz, B.; Antus, S.; Kurtán, T. X-ray structure determination, absolute configuration and biological activity of phomoxanthone A. *Eur. J. Org. Chem.* **2005**, *21*, 4563–4570. [CrossRef]

17. Rönsberg, D.; Debbab, A.; Mándi, A.; Vasylyeva, V.; Böhler, P.; Stork, B.; Engelke, L.; Hamacher, A.; Sawadogo, R.; Diederich, M.; et al. Pro-apoptotic and immunostimulatory tetrahydroxanthone dimmers from the endophytic fungus Phomopsislongicolla. *J. Org. Chem.* **2013**, *78*, 12409–12425. [CrossRef] [PubMed]

18. Cao, L.; Qiu, Z.; You, J.; Tan, H.; Zhou, S. Isolation and characterization of endophytic streptomycete antagonists of fusarium wilt pathogen from surface-sterilized banana roots. *FEMS Microbiol. Lett.* **2005**, *247*, 147–152. [CrossRef] [PubMed]

19. Frisch, M.J.; Trucks, G.W.; Schlegel, H.B.; Scuseria, G.E.; Robb, M.A.; Cheeseman, J.R.; Scalmani, G.; Barone, V.; Mennucci, B.; Petersson, G.A.; et al. *Gaussian 09*; revision a.02; Gaussian Inc.: Wallingford, CT, USA, 2009.

20. Bruhn, T.; Schaumloffel, A.; Hemberger, Y.; Bringmann, G. SpecDis: Quantifying the comparison of calculated and experimental electronic circular dichroism spectra. *Chirality* **2013**, *25*, 243–249. [CrossRef] [PubMed]

21. Stephens, P.J.; Harada, N. ECD cotton effect approximated by the Gaussian curve and other methods. *Chirality* **2010**, *22*, 229–233. [CrossRef] [PubMed]

22. Van Zandt, M.C.; Jones, M.L.; Gunn, D.E.; Geraci, L.S.; Jones, J.H.; Sawicki, D.R.; Sredy, J.; Jacot, J.L.; Dicioccio, A.T.; Petrova, T.; et al. Discovery of 3-[(4,5,7-trifluorobenzothiazol-2-yl)methyl]indole-*N*-acetic acid (lidorestat) and congeners as highly potent and selective inhibitors of aldose reductase for treatment of chronic diabetic complications. *J. Med. Chem.* **2005**, *48*, 3141–3152. [CrossRef] [PubMed]

23. Dolomanov, O.V.; Bourhis, L.J.; Gildea, R.J.; Howard, J.A.K.; Puschmann, H. *OLEX2:* A complete structure solution, refinement and analysis program. *J. Appl. Cryst.* **2009**, *42*, 339–341. [CrossRef]

24. Burla, M.C.; Caliandro, R.; Camalli, M.; Carrozzini, B.; Cascarano, G.L.; De Caro, L.; Giacovazzo, C.; Polidori, G.; Spagna, R. SIR2004: An improved tool for crystal structure determination and refinement. *J. Appl. Cryst.* **2005**, *38*, 381–388. [CrossRef]

25. Sheldrick, G.M. A short history of SHELX. *Acta Cryst.* **2008**, *A64*, 112–122. [CrossRef] [PubMed]

26. Ellman, G.L.; Courtney, K.D.; Andres, J.V.; Featherstone, R.M. A new and rapid colorimetric determination of acetylcholinesterase activity. *Biochem. Pharmacol.* **1961**, *7*, 88–92. [CrossRef]

27. Zhang, C.Y.; Wu, W.H.; Wang, J.; Lan, M.B. Antioxidant properties of polysaccharide from the brown seaweed *Sargassum graminifolium* (Turn.), and its effects on calcium oxalate crystallization. *Mar. Drugs* **2012**, *10*, 119–130. [CrossRef] [PubMed]

28. Wu, C.; Wang, L.; Fang, Z.; Hu, Y.; Chen, S.; Sugawara, T.; Ye, X. The Effect of the Molecular Architecture on the Antioxidant Properties of Chitosan Gallate. *Mar. Drugs* **2016**, *14*, 95. [CrossRef] [PubMed]

29. Kelman, D.; Posner, E.K.; McDermid, K.J.; Tabandera, N.K.; Wright, P.R.; Wright, A.D. Antioxidant activity of Hawaiian marine algae. *Mar. Drugs* **2012**, *10*, 403–416. [CrossRef] [PubMed]

30. Harasit, K.M.; Tapas, M.; Ambikesh, M. Kinetics of the basic hydrolysis of *tris* (1,10-phenenthroline) Fe (II): Influence of polymer-surfactant interactions. *Colloid Surf. A-Physicochem. Eng. Asp.* **2011**, *380*, 300–307.

31. Moradi-Afrapoli, F.; Asghari, B.; Saeidnia, S.; Ajani, Y.; Mirjani, M.; Malmir, M.; Dolatabadi Bazaz, R.; Hadjiakhoondi, A.; Salehi, P.; Hamburger, M.; et al. In vitro α-glucosidase inhibitory activity of phenolic constituents from aerial parts of *Polygonum hyrcanicum*. *Daru* **2012**, *20*, 37. [CrossRef] [PubMed]

32. Pierce, C.G.; Uppuluri, P.; Tristan, A.R.; Wormley, F.L., Jr.; Mowat, E.; Ramage, G.; Lopez-Ribot, J.L. A simple and reproducible 96-well plate-based method for the formation of fungal biofilms and its application to antifungal susceptibility testing. *Nat. Protoc.* **2008**, *3*, 1494–1500. [CrossRef] [PubMed]

33. Debbab, A.; Aly, A.H.; Proksch, P. Endophytes and associated marine derived fungi-ecological and chemical perspectives. *Fungal Divers.* **2012**, *57*, 45–83. [CrossRef]

34. Imhoff, J.F. Natural Products from Marine Fungi-Still an Underrepresented Resource. *Mar. Drugs* **2016**, *14*, 19. [CrossRef] [PubMed]

35. Wen, L.; Cai, X.; Xu, F.; She, Z.; Chan, W.L.; Vrijmoed, L.L.; Jones, E.B.; Lin, Y. Three metabolites from the mangrove endophytic fungus *Sporothrix* sp. (#4335) from the South China Sea. *J. Org. Chem.* **2009**, *74*, 1093–1098. [PubMed]

36. Ma, Y.H.; Li, J.; Huang, M.X.; Liu, L.; Wang, J.; Lin, Y.C. Six New Polyketide Decalin Compounds from Mangrove Endophytic Fungus *Penicillium aurantiogriseum* 328#. *Mar. Drugs* **2015**, *13*, 6306–6318. [PubMed]

37. Li, J.; Xue, Y.Y.; Yuan, J.; Lu, Y.J.; Zhu, X.; Lin, Y.C.; Liu, L. Lasiodiplodins from Mangrove Endophytic Fungus *Lasiodiplodia* sp. 318#. *Nat. Prod. Res.* **2015**, *30*, 1–6.